Revised Version

DESY 95-206
CERN-TH/95-315
ITP-Budapest Rep. No. 514

DESY 95-206
CERN-TH/95-315
ITP-Budapest Rep. No. 514

Numerical tests of the electroweak phase transition and thermodynamics of the electroweak plasma

F. Csikor
Institute for Theoretical Physics, Eötvös University,
Budapest, Hungary

Z. Fodor*
Theory Division, CERN, CH-1211 Geneva 23, Switzerland

J. Hein, A. Jaster, I. Montvay
Deutsches Elektronen-Synchrotron DESY,
Notkestr. 85, D-22603 Hamburg, Germany

hep-lat/9601016 10 May 1996

Abstract

The finite temperature phase transition in the SU(2) Higgs model at a Higgs boson mass $M_H \simeq 34$ GeV is studied in numerical simulations on four-dimensional lattices with time-like extensions up to $L_t = 5$. The effects of the finite volume and finite lattice spacing on masses and couplings are studied in detail. The errors due to uncertainties in the critical hopping parameter are estimated. The thermodynamics of the electroweak plasma near the phase transition is investigated by determining the relation between energy density and pressure.

*On leave from Institute for Theoretical Physics, Eötvös University, Budapest, Hungary.

1 Introduction

The electroweak phase transition [1] plays an important rôle in the baryon asymmetry of the Universe [2]. Since near the phase transition and in the phase with restored symmetry infrared singularities render the perturbation theory uncertain, non-perturbative numerical simulations may be very useful in providing numerical control of the perturbative resummation techniques [3, 4, 5, 6].

The present paper is a continuation of our previous work on this subject [7, 8, 9]. Our main goal is to test different sources of systematic errors in four-dimensional simulations. The value of the Higgs boson mass $M_H \simeq 34\ GeV$ is chosen such that comparisons of our four-dimensional results with three-dimensional work in reduced models [10, 11, 12, 13] become possible. The dimensional reductional technique can be used to test classes of electroweak phase transition models; however, the quality of the approximation should be controlled. The hope is that for Higgs boson masses between 20 GeV and 80 GeV the combined outcome of resummed perturbation theory and of unreduced and reduced numerical simulations will be a complete understanding of the thermodynamics of the electroweak phase transition. (For a recent review of the subject, see e. g. [14].) In fact, in the present paper we also do a first step towards the determination of the thermodynamical equations of state in the electroweak plasma, by investigating the relation between energy density and pressure on both sides of the phase transition (for $1/4 \leq T/T_c \leq 2$).

The notations in the present paper are the same as in our previous works [7, 8, 9]. For the reader's convenience we repeat here the lattice action:

$$S[U,\varphi] = \beta \sum_{pl} \left(1 - \frac{1}{2}\mathrm{Tr}\, U_{pl}\right)$$

$$+ \sum_x \left\{ \frac{1}{2}\mathrm{Tr}\,(\varphi_x^+ \varphi_x) + \lambda \left[\frac{1}{2}\mathrm{Tr}\,(\varphi_x^+ \varphi_x) - 1\right]^2 - \kappa \sum_{\mu=1}^{4} \mathrm{Tr}\,(\varphi_{x+\hat{\mu}}^+ U_{x\mu} \varphi_x) \right\} . \qquad (1)$$

Here $U_{x\mu}$ denotes the SU(2) gauge link variable, U_{pl} is the product of four U's around a plaquette, and φ_x is a complex $2 \otimes 2$ matrix in isospin space describing the Higgs scalar field. The bare parameters in the action are $\beta \equiv 4/g^2$ for the gauge coupling, λ for the scalar quartic coupling and κ for the scalar hopping parameter related to the bare mass square μ_0^2 by $\mu_0^2 = (1 - 2\lambda)\kappa^{-1} - 8$. In what follows we set the lattice spacing to 1 ($a = 1$), therefore all the masses and correlation lengths, etc., will always be given in lattice units, unless otherwise stated.

The numerical simulations were performed on the APE-Quadrics parallel computers at DESY-Zeuthen. In order to obtain the desired value of the Higgs boson mass ($M_H \simeq 34$ GeV), we had to choose for the bare quartic coupling $\lambda \simeq 0.0003$. The other two bare couplings are in the same range as for the previously studied cases: $\lambda \simeq 0.0001,\ 0.0005$ (corresponding to $M_H \simeq 18,\ 50$ GeV, respectively). The lattice extents in time (i. e. inverse temperature)

direction were in the range $2 \leq L_t \leq 5$. For the determination of the thermodynamical equation of state we used $L_t = 2$ and 4. These choices of L_t allowed us to estimate the magnitude of the lattice discretization errors, too.

The simulation algorithms have been described in detail in our previous publications. An important ingredient for reducing the autocorrelations of the generated field configurations is the overrelaxation algorithm for the Higgs field [15]. The numerical tests in our parameter range showed that the best variant is the one proposed in [16]. For instance, comparing the methods of [15] and [16] on a $12^3 \cdot 32$ lattice with $\beta = 8.0$, $\kappa = 0.1287$ and $\lambda = 0.0003$ the method of [16] reduced the integrated autocorrelation time for the length of the Higgs field from 7.4 sweeps to 0.9 sweeps. The speed-up factor in CPU-time is about 14, because the algorithm in [16] is simpler.

The plan of this paper is as follows: First, in the next section, the finite volume effects on masses and couplings are discussed. The errors of the critical hopping parameter and their effects on the determination of the latent heat are investigated in section 3, whereas section 4 is devoted to the thermodynamics of the electroweak plasma. In section 5 our results are compared to two-loop resummed perturbation theory. Finally, the last section contains the discussion of the results and future plans.

2 Finite volume and finite lattice spacing effects

In this section we discuss the finite volume and finite lattice spacing effects on the zero temperature renormalized quantities, i. e. the masses and the gauge coupling.

2.1 Zero temperature masses

As in refs. [7, 8], the physical Higgs mass M_H was extracted from correlators of the following quantities:

$$R_x \equiv \frac{1}{2}\mathrm{Tr}(\varphi_x^+ \varphi_x) \equiv \rho_x^2 \,, \tag{2}$$

and, using $\varphi_x \equiv \rho_x \alpha_x$ with $\alpha_x \in \mathrm{SU}(2)$,

$$L_{\alpha,x\mu} \equiv \frac{1}{2}\mathrm{Tr}(\alpha_{x+\hat{\mu}}^+ U_{x\mu}\, \alpha_x) \,, \qquad L_{\varphi,x\mu} \equiv \frac{1}{2}\mathrm{Tr}(\varphi_{x+\hat{\mu}}^+ U_{x\mu}\, \varphi_x) \,. \tag{3}$$

The W-boson mass M_W was obtained from the correlator of the composite link fields

$$W_x \equiv \sum_{r,k=1}^{3} \frac{1}{2}\mathrm{Tr}(\tau_r \alpha_{x+\hat{k}}^+ U_{xk}\, \alpha_x) \,. \tag{4}$$

Simulations to determine the zero temperature masses were performed on several lattices of different space extensions at the phase transition point of the $L_t = 2$ lattice. For $L_t = 3, 4, 5$ the lattice volumes were chosen large enough, to be close to the infinite volume limit. The simulation parameters are collected in table 1. Besides the simulation points close to the

Table 1: *The parameter values of numerical simulations for the determination of zero temperature masses and renormalized gauge couplings. The indices for the four sets of simulation points* m2, m3, m4 *and* m5 *correspond to* $L_t = 2, 3, 4$ *and* 5*, respectively. The numbers in brackets refer to the linear size of the lattice and to the last two digits of the hopping parameter.*

index	lattice	β	κ	λ	sweeps	subsamples
m2[6]	$6^3 \cdot 32$	8.00	0.12865	0.0003	384000	64
m2[8]	$8^3 \cdot 32$	8.00	0.12865	0.0003	288000	16
m2[12/65]	$12^3 \cdot 32$	8.00	0.12865	0.0003	320000	80
m2[16]	$16^3 \cdot 32$	8.00	0.12865	0.0003	192000	96
m2[24]	$24^3 \cdot 64$	8.00	0.12865	0.0003	38000	20
m2[12/70]	$12^3 \cdot 32$	8.00	0.12870	0.0003	448000	32
m3[24/35]	$24^3 \cdot 32$	8.15	0.128355	0.00031	32000	80
m3[24/40]	$24^3 \cdot 32$	8.15	0.128405	0.00031	11200	28
m4[24/35]	$24^3 \cdot 64$	8.25	0.128235	0.000315	168000	28
m4[24/85]	$24^3 \cdot 64$	8.25	0.128285	0.000315	14400	36
m5[32/17]	$32^3 \cdot 64$	8.33	0.128170	0.000319	37740	74
m5[32/21]	$32^3 \cdot 64$	8.33	0.128210	0.000319	15300	30

critical hopping parameter there are also points with shifted κ, in order to control the effects of uncertainties in the critical hopping parameter.

Masses were extracted from the correlators fitting to a cosh+constant function. Simple uncorrelated least square fits and correlated fits (eventually with eigenvalue smoothing) [17] were used. The use of the latter method (Michael–McKerrell method) is necessary, since the data are strongly correlated for different time distances.

For the reader's convenience – following [17] – we briefly define how to perform correlated and Michael–McKerrell fits. Let us denote the measured data of a correlator by $x^{(n)}(t)$, with t the time difference ($t = t_0 + 1 \ldots t_0 + D$). We assume N data samples (i. e. $n = 1 \ldots N$), with averages $\overline{X}(t)$. Our aim is to fit our data to a given function $F(t, a)$, which depends on P parameters $a \equiv a_1, \ldots, a_P$. To find the best fit parameters corresponds to minimizing with respect to a

$$\chi^2 = \sum_{t,t'} (F(t,a) - \overline{X}(t)) M(t,t') (F(t',a) - \overline{X}(t')) \ , \tag{5}$$

where

$$\overline{X}(t) = \frac{1}{N} \sum_{n=1}^{N} x^{(n)}(t) \ , \tag{6}$$

$$M(t,t') = N C^{-1}(t,t') \ , \tag{7}$$

with

$$C(t,t') = \frac{1}{N-1}\sum_{n=1}^{N}(x^{(n)}(t) - \overline{X}(t))(x^{(n)}(t') - \overline{X}(t')) \ . \tag{8}$$

The uncorrelated fit corresponds to ignoring non-diagonal elements in the correlation matrix $C(t,t')$.

The difficulty is that the elements of the inverse correlation matrix have a tendency to get large statistical errors. To deal with this problem, the Michael–McKerrell method proposes to change the D eigenvalues λ_i of the normalized correlation matrix

$$\tilde{C}(t,t') = \frac{C(t,t')}{\sqrt{C(t,t)C(t',t')}} \tag{9}$$

as follows:

$$\lambda_i^{'} = K \ \max(\lambda_i, \lambda_{min}) \ , \tag{10}$$

where

$$\lambda_{min} = \frac{1}{D-E}\sum_{i=E+1}^{D}\lambda_i \ , \qquad K^{-1} = \frac{1}{D}\sum_{i=1}^{D} \ \max(\lambda_i, \lambda_{min}) \ . \tag{11}$$

It is assumed that the eigenvalues λ_i are arranged in decreasing order. The eigenvectors of $\tilde{C}(t,t')$ and thus of its inverse $\tilde{M}(t,t')$ are retained unchanged. The procedure removes any very small eigenvalues of $\tilde{C}(t,t')$ and replaces them with the average of the $D-E$ smallest eigenvalues while retaining the property that the trace of $\tilde{C}(t,t')$ is D. From the practical tests it is suggested that E should be about $\sqrt{N}$.

The advantage of the correlated (or Michael–McKerrell) method is twofold. First, the values of χ^2 per degree of freedom obtained by the uncorrelated least square fits are notoriously low, thus making impossible the choice of the reasonable fit interval. Performing a correlated fit or its Michael–McKerrell extension, the χ^2/d.o.f. is reasonable, i. e. the best value is near unity. The second advantage is obtained when the statistics and the number of subsamples is low. In this case the correlation matrix $\tilde{C}(t,t')$ may have very low eigenvalues, which influences unreasonably the inverse of the correlation matrix used in modelling the distribution of the data. The proposal of [17] is to smear the smallest eigenvalues. It turns out that the method results in reasonable χ^2/d.o.f values even in such cases. Examples illustrating the above statements are given in tables 2 and 3.

In order to perform the correlated (and Michael–McKerrell) fits, the data were subdivided into subsamples. The errors on the data in the subsamples are not used in these fits. The errors of the data in the total data sample (used in the uncorrelated fits) were determined from the statistical fluctuations of subsample data or the errors of the subsample's data. The statistical errors of masses obtained in the fits were determined by jackknife analyses.

The actual procedure of extracting the mass parameters is the following. First one determines the reasonable intervals for fitting the data. The guideline is to choose as large an interval as possible with reasonable χ^2/d.o.f. value. For this purpose correlated fits with eigenvalue smearing were used. The *best fit* value of the masses was taken to be the number given by

Table 2: *Comparison of the uncorrelated fit (index I) and correlated fit (index II) for the $16^3 \cdot 32$ lattice (ρ_x^2 correlator), with data divided into 96 subsamples. The 0–16 interval is obviously excluded by the correlated fit, while superficially the uncorrelated fit seems to be reasonable.*

interval	Higgs mass I	$\chi^2/d.o.f.$ I	Higgs mass II	$\chi^2/d.o.f.$ II
2–8	0.24027	$1.072 \cdot 10^{-3}$	0.24207	1.08
2–10	0.23989	$1.494 \cdot 10^{-3}$	0.24277	1.08
2–12	0.24073	$5.71 \cdot 10^{-3}$	0.24283	1.01
2–14	0.24265	$2.48 \cdot 10^{-3}$	0.24272	0.965
2–16	0.24369	$5.92 \cdot 10^{-3}$	0.24327	0.992
0–16	0.24601	0.209	0.26242	59.13

the uncorrelated fit. In case of the Higgs mass, where three different correlators were measured, the final value of the Higgs mass was obtained by averaging the individual fit results. The errors on the masses were determined by jackknife analysis. The masses obtained by the correlated fits with eigenvalue smearing are in all cases well within the error bars of the uncorrelated fits. Thus the uncertainty of the choice of the best fit value is not too important. An additional uncertainty is caused by the choice of the fit interval. Even though it seems reasonable to include as many points as allowed by the χ^2/d.o.f., this is not compulsory. One may e. g. take the intervals with smallest χ^2/d.o.f.'s. Again the additional uncertainty caused by such a choice of the interval is not really important.

Our results are summarized in table 4. The first 5 rows there refer to the same physical situation, only the lattice sizes are different. Thus the data are suitable to demonstrate finite size effects. One observes that the masses and the Higgs to W-boson mass ratio (R_{HW}) are different for the $6^3 \cdot 32$ lattice as compared to the larger ones. The larger lattices yield, within errors, equal masses and R_{HW}, thus finite size effects are already small for these lattices. (In case of the $24^3 \cdot 64$ lattice, the errors are much larger than for the other lattices.)

Comparing the points with slightly shifted κ but otherwise same parameters one observes that the masses are changed; however R_{HW} remains unchanged within errors.

For the parametrization of the volume dependence of masses one can apply a formula suggested by the large volume asymptotic behaviour in scalar field theory [18]. Here we only want to illustrate the qualitative behaviour, therefore we omit possible power corrections, and for spatial lattice extent L_s assume the behaviour

$$M(L_s) \simeq M(\infty)[1 - c \exp(-L_s m)] \ . \tag{12}$$

This is a three-parameter form, with the infinite volume mass $M(\infty)$, the constant c and the exchange mass parameter m. Since the number of points in L_s is not much larger than the

Table 3: *Comparison of the correlated fits with different numbers of smeared eigenvalues of the correlation matrix for the $24^3 \cdot 64$ lattice (ρ^2 correlator), with data divided into 20 subsamples. The fit interval is 2–26, so there are 6 zero eigenvalues. Inversion of the correlation matrix is impossible, smearing of the lowest eigenvalues is necessary. The last row (5 exact eigenvalues retained) gives quite a reasonable fit.*

interval	smeared eigenvalues	Higgs mass	$\chi^2/d.o.f.$
2–26	7	0.24573	266.9
2–26	8	0.24609	34.79
2–26	10	0.24571	6.25
2–26	12	0.24518	3.88
2–26	14	0.24727	2.88
2–26	16	0.24643	1.79
2–26	18	0.24570	1.87
2–26	20	0.24361	1.75

number of parameters, the only question is the qualitative description with a reasonable set of parameters. In fact, within our range of L_s and statistical errors the Higgs boson mass is constant. This is illustrated by figure 1. For the W-boson mass a reasonable fit of the form (12) can be obtained (see figure 2). In this case the value of the exchange mass m comes out, as expected, not much different from the Higgs mass M_H.

2.2 Renormalized gauge coupling

The renormalized gauge coupling was determined in the usual way from the static potential [8]. The potential as a function of the distance R was fitted by

$$V(R) = -\frac{A}{R} e^{-MR} + C + D\, G(M, R, L_s) \ , \tag{13}$$

where the last term with $G(M, R, L_s)$ corrects for lattice artefacts. The value of the potential at R was obtained from the rectangular Wilson loops by fitting the time dependence with three exponentials. The high statistics for the Wilson loops allowed a stable fit with good χ^2 if the smallest time distances, between one at $L_t = 3$ and three at $L_t = 5$, were omitted. The potential was then fitted by the form in (13). For $L_t = 2$ every R-value was used, but for $3 \leq L_t \leq 5$ the first point with $R = 1$ contributed too much to χ^2. The discrepancy was increasing for increasing L_t. Fitting only $R \geq 2$ the value of the fit curve at $R = 1$ deviated from the measured one by about hundred standard deviations. Therefore the formula (13) is clearly not valid for $L_t \geq 3$ and $R = 1$. The tree-level perturbative correction for lattice artefacts $G(M, R, L_s)$ is

Table 4: *Final results on the Higgs and W masses. The lattices are in the same order as above in table 1 for simulation parameters and are identified by the indices defined there. Higgs and W masses are first given in lattice units.* $R_{HW} = M_H/M_W$.

index	interval	M_H	interval	M_W	R_{HW}	M_H (GeV)
m2[6]	2 – 16	0.2336(13)	2 – 16	0.5587(13)	0.4181(33)	33.5
m2[8]	2 – 16	0.2480(12)	3 – 11	0.5573(28)	0.4450(44)	35.7
m2[12/65]	2 – 16	0.2451(14)	2 – 16	0.5619(21)	0.4362(41)	35.0
m2[16]	2 – 16	0.2436(21)	2 – 16	0.5644(21)	0.4316(53)	34.6
m2[24]	2 – 32	0.2471(39)	2 – 22	0.5665(17)	0.436(8)	35.0
m2[12/70]	2 – 16	0.2585(9)	2 – 16	0.5888(13)	0.4390(25)	35.2
m3[24/35]	2 – 32	0.1587(14)	2 – 32	0.3712(31)	0.428(7)	34.2
m3[24/40]	2 – 32	0.1796(40)	2 – 32	0.414(8)	0.433(18)	34.7
m4[24/35]	2 – 32	0.1198(15)	4 – 32	0.2765(23)	0.433(9)	34.8
m4[24/85]	2 – 32	0.1428(25)	2 – 32	0.3427(42)	0.417(12)	33.4
m5[32/17]	2 – 32	0.0907(15)	4 – 32	0.221(5)	0.411(16)	32.9
m5[32/21]	2 – 32	0.1205(20)	2 – 32	0.284(5)	0.425(15)	34.0

not good enough for our high precision data. Omitting also $R = 2$ and fitting only for $R \geq 3$ gave already compatible results with $R \geq 2$. Hence the fits for $3 \leq L_t \leq 5$ were done with $R \geq 2$.

All results are collected in table 5, with the point indices given in table 1. The point m2[6] was omitted, because at least $L_s = 8$ is required to fit four parameters. Obviously, finite size effects for the renormalized gauge coupling and the screening mass are small. The reason is that the values of these parameters are determined from the behaviour of the potential at small distances. Only the constant C, which is given by the asymptotic dependence, shows larger finite size effects. The global (g_R^2) and local ($g_R^2(M^{-1})$) gauge couplings (defined e. g. in [8]) and the constant C as a function of the space extention L_s are shown in figs. 3 and 4. The volume dependence of the W-boson mass parameter M obtained from the static potential is comparable with that of the pole mass M_W. This is shown in figure 5, where a fit of the same form as in eq. (12) is plotted. The values of the three fit parameters are roughly the same as those for M_W in figure 2.

In summary, the finite size effects on our zero temperature lattices are small. For instance, at the phase transition point of the $L_t = 2$ lattices the values of the Higgs-boson and W-boson masses as well as those of the renormalized gauge coupling are on lattices with spatial extension 12^3 equal within errors to the values on 16^3 and 24^3. Therefore, these latter lattice sizes can be considered, within our small statistical errors, to represent the infinite volume situation. This

Table 5: *Summary of the fit parameters for the static potential and the renormalized gauge coupling.*

index	A	M	D	C	$g_R^2 \equiv \frac{16}{3}\pi A$	$g_R^2(M^{-1})$
m2[8]	0.03415(11)	0.538(4)	0.0336(7)	0.08673(5)	0.5722(19)	0.571(3)
m2[12/65]	0.03422(3)	0.5498(14)	0.0356(5)	0.086177(6)	0.5734(5)	0.5764(16)
m2[16]	0.03427(3)	0.5551(13)	0.0366(6)	0.086117(3)	0.5741(5)	0.5788(16)
m2[24]	0.03430(9)	0.555(4)	0.0361(18)	0.086115(6)	0.5747(15)	0.578(3)
m2[12/70]	0.03420(3)	0.5815(14)	0.0360(5)	0.085050(5)	0.5731(5)	0.5764(13)
m3[24/35]	0.0367(11)	0.378(7)	0.026(4)	0.091716(12)	0.615(18)	0.591(7)
m3[24/40]	0.0354(23)	0.413(13)	0.031(9)	0.090100(15)	0.602(38)	0.583(10)
m4[24/35]	0.0353(6)	0.269(5)	0.0293(24)	0.094267(19)	0.592(10)	0.584(6)
m4[24/85]	0.0352(10)	0.328(7)	0.030(4)	0.092065(21)	0.590(17)	0.580(8)
m5[32/17]	0.0354(5)	0.2135(35)	0.0275(22)	0.095416(20)	0.593(8)	0.586(8)
m5[32/21]	0.0352(7)	0.270(5)	0.028(3)	0.093295(22)	0.590(12)	0.581(8)

information obtained on $L_t = 2$ lattices can be used, by scaling up L_s with L_t, to choose the spatial lattice size of $L_t \geq 3$ lattices sufficiently large, in order to avoid finite volume effects.

Another important question is the size of lattice artefacts. These are expected to be of the order $\mathcal{O}(1/L_t^2)$, hence decrease by a factor 4/25 between $L_t = 2$ and $L_t = 5$. Our points with increasing L_t were chosen on a line of constant physics (LCP) using the one-loop β-functions [8]. Along such lines R_{HW} and $g_R^2(M^{-1})$ should be constant. An investigation of tables 4 and 5 shows that, within errors, this is indeed the case: all values at the critical hopping parameter on large lattices agree with $R_{HW} = 0.422(11)$ and $g_R^2(M^{-1}) = 0.585(10)$. At the same time the masses scale properly by $1/L_t$. In addition, the physical fit parameters in the potential, namely $g_R^2(M^{-1})$ and M/M_W are also constant within errors, therefore also the physical shape of the potential scales. It is also true that the mass parameter M obtained from the static potential is equal to the pole mass M_W of the W boson. In fact, the good scaling of the masses and static potential already at $L_t = 2$ is surprising. Since our errors are at the level of 1-2%, the magnitude of lattice artefacts in R_{HW} and $g_R^2(M^{-1})$ on $L_t = 5$ lattices is at the level of a few parts per thousand.

3 Critical hopping parameter and latent heat

An important step in numerical simulations is the determination of the critical hopping parameter κ_c on lattices with high temperatures, where the first order phase transition between the Higgs phase and the symmetric phase (i. e. phase with restored symmetry) occurs. On lattices

with finite spatial volumes there is some uncertainty concerning the exact definition of this critical hopping parameter value. Usually, different possible definitions, as the equal area or equal height criterion in different order parameter distributions, give slightly different values. For growing volumes this uncertainty goes rapidly (in most cases exponentially) to zero, but in finite volumes this constitutes an inherent uncertainty. In addition, the statistical errors of the numerical simulations also increase the errors of κ_c.

This error propagates to other physical quantities as, for instance, latent heat. The reason for this is that the uncertainty in the knowledge of the exact position of the transition point leads to additional uncertainties in the magnitude of the jump of order parameters like ΔP_{pl}, $\Delta L_{\varphi,x\mu}$, etc. In order to control this kind of errors, in the present section we discuss how to determine the κ-dependence of the order parameters in a fairly wide κ-range from the results of a single run. In the determination of the latent heat, this procedure is used for a refined error analysis.

3.1 Critical point and renormalization group trajectories

As discussed in refs. [7, 8], the knowledge of the critical hopping parameters can be directly used to determine the renormalization group trajectories or *lines of constant physics* (LCP's). The derivatives of the bare parameters along LCP's also appear in the formula for the latent heat (see section 3.3).

For the flow of the bare couplings β and λ along the lines of constant physics we used the one-loop perturbative renormalization group equation as already described in refs. [7, 8]. In order to determine the critical hopping parameters, two different approaches were applied. For $L_t = 2$ we used the more precise constrained simulation, for which κ_c is defined by the flat distribution of an order parameter between the two peaks of the first order phase transition. The method and the result are published in ref. [9]. For the sake of completeness, we just quote the result for κ_c. This method was not applicable in the case of the larger L_t-values, because it requires 64-bit numerical precision, which is missing on the APE-Quadrics computer. The CRAY-YMP at HLRZ Jülich has the necessary precision, but due to memory restrictions we were not able to perform the simulations on large volumes, corresponding to $L_t = 4$. Therefore the two-coupling method described in refs. [21, 8] was used for $L_t > 2$. This method devides the lattice into two halves. In one half $\kappa_1 < \kappa_c$, in the other one $\kappa_2 > \kappa_c$. Demanding two bulk phases and two interfaces one receives upper and lower bounds for κ_c. This is rather robust and simple but, of course, in the 32-bit arithmetics of APE-Quadrics it gives less precision. The obtained values for the critical hopping parameter κ_c are given in table 6.

At the phase transition points the temporal extension of the lattice is equal to the inverse transition temperature in lattice units: $L_t = 1/T_c$. On a given LCP the ratio $M_W/T_c = M_W L_t$ is constant, therefore the change of the scale parameter $\tau \equiv -\log(M_W)$ between $L_t = L_t^{(1)}$ and $L_t = L_t^{(2)}$ is given by $\Delta\tau \equiv \tau^{(2)} - \tau^{(1)} = \log(L_t^{(2)}/L_t^{(1)})$. Since the lattice spacing is set to $a = 1$,

Table 6: *Critical hopping parameters.*

lattice	β	λ	κ_c	method
$2{\cdot}24^2{\cdot}256$	8.0	0.0003	0.1286565(7)	constrained
$3{\cdot}32^2{\cdot}512$	8.15	0.00031	0.128355(5)	2-coupling
$4{\cdot}44^2{\cdot}512$	8.25	0.000315	0.128235(5)	2-coupling
$5{\cdot}56^2{\cdot}560$	8.33	0.000319	0.128170(5)	2-coupling

τ characterizes the lattice resolution. With increasing τ the continuum limit is approached.

The derivative of the hopping parameter with respect to τ along the LCP's can be obtained from polynomial interpolations of the simulation data for κ_c on lattices with different time extensions L_t. Here we consider lattices with $2 \leq L_t \leq 5$. In order to determine the statistical errors of the derivatives, the polynomial interpolations were repeated with 500 normally distributed random values around the measured mean values. An estimate of the systematic errors can be obtained by comparing 2nd- and 3rd-order interpolations. The resulting values for $\partial\kappa/\partial\tau$ including both types of errors are:

$$\left.\frac{\partial\kappa}{\partial\tau}\right|_{\mathrm{m2}} = -1.00(10)\cdot 10^{-3}, \qquad \left.\frac{\partial\kappa}{\partial\tau}\right|_{\mathrm{m3}} = -0.53(4)\cdot 10^{-3}, \qquad \left.\frac{\partial\kappa}{\partial\tau}\right|_{\mathrm{m4}} = -0.34(2)\cdot 10^{-3}\ . \quad (14)$$

3.2 Uncertainties of the critical point and order parameters

As noted above, the uncertainties of the critical hopping parameters contribute to the errors of some other physical quantities. The variation of global quantities (e. g. average link) leads to an important uncertainty in the determination of the latent heat. In principle, the dependence of these global quantities on κ can be determined in a single run by κ-reweighting [20]. This works well, if the κ-shifts are so small that the corresponding shifts of the measured quantities are smaller than their variances. However, in our case, due to the large lattice volumes, the allowed κ-shifts turned out to be too small. To come around this problem, we performed Taylor fits to the data obtained from reweighting and used the obtained Taylor series extrapolations to estimate the quantities at the required κ's.

We checked this procedure for the link variable by performing simulations with different κ's on a $2 \cdot 32 \cdot 32 \cdot 196$ lattice at $\beta = 8.0$, $\lambda = 0.0003$. The values of the hopping parameter were $\kappa = 0.12865$ and $\kappa = 0.12866$, respectively. Both of these points are in the metastable range. The lattice configurations were set into the Higgs phase. At $\kappa = 0.12866$ we used reweighting to nearby κ values. The result of the reweighting and the Taylor fits for the quantity $L_{\varphi,x\mu}$ is given in fig. 6. The statistical errors of the Taylor coefficients and of the estimates at the required κ-values were determined by a bootstrap procedure [22, 9] with 32 data blocks.

Figure 6 shows that the first-order fit is insufficient to reproduce the result of the direct

measurement at $\kappa = 0.12865$. The second-order fit is in reasonably good agreement with the direct value, and the third-order fit gives only an insignificant change. This holds for the quantities P_{pl} and Q_x as well. Repeating this procedure in the symmetric phase, reasonable agreement within errors was found too. Therefore, also in other points the Taylor series was used up to the last significant coefficient.

3.3 Latent heat

As it has been already discussed in ref. [8], the latent heat $\Delta\epsilon$ can be obtained from the discontinuity of $\delta \equiv \epsilon/3 - P$, where ϵ and P denote energy density and pressure, respectively. This implies that $\Delta\epsilon$ can be determined from the jumps of some order parameters by

$$\frac{\Delta\epsilon}{T_c^4} = L_t^4 \left(8\frac{\partial\kappa}{\partial\tau}\langle\Delta L_{\varphi,x\mu}\rangle - \frac{\partial\lambda}{\partial\tau}\langle\Delta Q_x\rangle - 6\frac{\partial\beta}{\partial\tau}\langle\Delta P_{pl}\rangle \right) \ . \tag{15}$$

The link variable is defined in (3), moreover

$$P_{pl} \equiv 1 - \tfrac{1}{2}\mathrm{Tr}\, U_{pl} \ , \qquad Q_x \equiv \left(\rho_x^2 - 1\right)^2 \ . \tag{16}$$

The results of the numerical simulations for the determination of the latent heat are given in table 7. The order parameters in the vicinity of the transition point were obtained by the method described in the previous subsection. Note the sensitivity of the Higgs phase results on the small deviations in κ.

The derivatives $\partial\lambda/\partial\tau$ and $\partial\beta/\partial\tau$ in eq. (15) were taken from the one-loop perturbative renormalization group equations. As discussed in section 2, the renormalized quantities show a good scaling between $L_t = 2$ and $L_t = 5$ according to the one-loop formulas. Therefore we neglected the uncertainties of $\partial\lambda/\partial\tau$ and $\partial\beta/\partial\tau$. Together with the results for $\partial\kappa/\partial\tau$ in eq. (14), we obtain

$$\left.\frac{\Delta\epsilon}{T_c^4}\right|_{\mathrm{m2}} = 0.240(30+4) \ , \qquad \left.\frac{\Delta\epsilon}{T_c^4}\right|_{\mathrm{m4}} = 0.28(3+9) \ . \tag{17}$$

The result with index m4 (temporal lattice extension $L_t = 4$) was obtained in the point with hopping parameter $\kappa_c = 0.128235$ corresponding to table 6. (In table 1 this point has the index m4[24/35].) The first number in parenthesis is the error originating from the uncertainties of $\partial\kappa/\partial\tau$ and the statistical errors quoted in table 7. The second one gives the influence of the error of the critical hopping parameter. In the case of $L_t = 4$ a more precise estimate of the critical hopping parameter is obviously desirable, in order to get a smaller error of the latent heat. Within the large errors, the result of the $L_t = 4$ lattice agrees with that of $L_t = 2$, and hence with scaling.

Table 7: *Global average quantities for the determination of δ and latent heat. The first part refers to $T_c = \frac{1}{2}$, the second one to $T_c = \frac{1}{4}$ (in lattice units). The bare parameters are $\beta = 8.0, \lambda = 0.0003$ and $\beta = 8.15, \lambda = 0.000315$, respectively. At the phase transition there are two points corresponding to the two metastable phases. The statistical errors are quoted in parentheses. The last entry in every column gives the variation of the quantity in last digits when κ is changed within its statistical error: $\kappa = 0.1286565(\pm 7)$ and $\kappa = 0.128235(\pm 5)$, respectively. The column "fit" specifies the order of the applied extrapolation.*

lattice	fit	P_{pl}	$L_{\varphi,x\mu}$	Q_x
$32{\cdot}32^2{\cdot}32$	1st order	$0.0919035(8)\mp 61$	$9.1869(9)\pm 130$	$132.124(21)\pm 300$
$8{\cdot}32^2{\cdot}32$	1st order	$0.0919075(7)\mp 61$	$9.1757(8)\pm 130$	$131.898(18)\pm 300$
$6{\cdot}32^2{\cdot}96$	1st order	$0.0919204(9)\mp 61$	$9.1298(11)\pm 130$	$130.888(25)\pm 300$
$5{\cdot}32^2{\cdot}96$	1st order	$0.0919557(10)\mp 61$	$9.0521(11)\pm 130$	$129.162(24)\pm 300$
$4{\cdot}32^2{\cdot}96$	1st order	$0.0920461(5)\mp 63$	$8.8239(5)\pm 130$	$124.103(10)\pm 300$
$3{\cdot}32^2{\cdot}96$	1st order	$0.0923641(5)\mp 70$	$8.0267(6)\pm 140$	$107.063(13)\pm 300$
$2{\cdot}32^2{\cdot}96$	2nd order	$0.094712(7)\mp 19$	$3.112(13)\pm 34$	$28.20(15)\pm 39$
$2{\cdot}32^2{\cdot}96$	2nd order	$0.0960210(6)\mp 3$	$0.9199(4)\pm 5$	$8.074(3)\pm 4$
$48{\cdot}48^2{\cdot}48$	1st order	$0.0923167(3)\mp 470$	$2.5434(5)\pm 950$	$21.199(5)\pm 930$
$12{\cdot}64^2{\cdot}64$	1st order	$0.0923226(4)\mp 490$	$2.5292(6)\pm 980$	$21.066(6)\pm 960$
$8{\cdot}64^2{\cdot}64$	1st order	$0.0923604(7)\mp 530$	$2.4571(10)\pm 1000$	$20.380(10)\pm 1000$
$6{\cdot}64^2{\cdot}192$	1st order	$0.0924439(6)\mp 500$	$2.2809(9)\pm 1000$	$18.734(8)\pm 940$
$5{\cdot}64^2{\cdot}192$	1st order	$0.0925683(6)\mp 590$	$2.0276(10)\pm 1200$	$16.467(9)\pm 1000$
$4{\cdot}64^2{\cdot}192$	2nd order	$0.0929636(11)^{-1000}_{+1300}$	$1.2440(23)^{+2000}_{-2400}$	$10.227(17)^{+1500}_{-1700}$
$4{\cdot}64^2{\cdot}192$	2nd order	$0.0933086(3)^{-28}_{+13}$	$0.5939(3)^{+57}_{-32}$	$5.955(2)^{+34}_{-19}$
$3{\cdot}64^2{\cdot}192$	2nd order	$0.0932657(4)^{-8}_{+3}$	$0.64536(7)\pm 110$	$6.2639(4)\pm 69$
$3{\cdot}92^2{\cdot}192$	2nd order	$0.0932655(6)\mp 10$	$0.64522(14)\pm 100$	$6.2630(9)\pm 63$
$2{\cdot}64^2{\cdot}192$	2nd order	$0.0930844(6)^{-7}_{+1}$	$0.83147(6)\pm 75$	$7.4490(4)\pm 52$

4 Relation between energy density and pressure

The thermodynamical quantity $\delta \equiv \epsilon/3 - P$, where ϵ is the energy density and P the pressure, has been used in section 3.3 for the determination of the latent heat. It is an interesting quantity on its own, because it reflects the deviation of the thermodynamical equations of state from those of a free relativistic massless gas (photon gas). In the latter case $\delta = 0$, thus $\epsilon/3 = P$. The reason why it is advantageous to extract the latent heat from the jump of δ at the phase transition is its relatively simple expression in terms of global averages on the lattice:

$$\delta = \frac{1}{3}(TL_t)^4 \left\langle \frac{\partial\kappa}{\partial\tau} \cdot 8L_{\varphi,x\mu} - \frac{\partial\lambda}{\partial\tau} \cdot Q_x - \frac{\partial\beta}{\partial\tau} \cdot 6P_{pl} \right\rangle \ . \tag{18}$$

Here T is the temperature corresponding to the temporal lattice extension L_t. The quantities $L_{\varphi,x\mu}$, Q_x, P_{pl} are defined in eqs. (3) and (16) and $\tau \equiv -\log(M_W)$ is the lattice scale parameter. The derivatives as $\partial\kappa/\partial\tau$ etc. are taken along the line of constant physics going through the point (β, λ, κ) in bare parameter space. The expression in eq. (18) still contains a divergent vacuum contribution, which has to be subtracted from the right-hand side. In numerical simulations the most convenient way is to subtract from the right-hand side the same expression on a lattice with large temporal extension corresponding to zero temperature. In this way one ends up with $\delta(T)/T^4$, because $\lim_{T\searrow 0} \delta(T)/T^4 = 0$.

Of course, it would be interesting to know δ as a function of the temperature. For instance, much above the phase transition temperature $T \gg T_c$ it can be expected, at least for small quartic coupling λ, that masses can be neglected and interactions are weak, which corresponds to $\delta(T)/T^4 \ll 1$. (Note that $\delta(T)/T^4$ is dimensionless.) Above the phase transition temperature the system is in the symmetric phase, where perturbation theory cannot be applied; therefore one has to rely on non-perturbative methods. In the Higgs phase, well below T_c, resummed perturbation theory should give a good description.

In a numerical simulation the simplest way to change the temperature is to change the temporal lattice extension L_t, which is proportional to the inverse temperature. Another possibility would be to change the lattice spacing in time direction for fixed L_t and spatial lattice spacing, but this would require the introduction of different gauge couplings and hopping parameters in the timelike and spacelike directions. We choose to change L_t and keep the parameters fixed. Therefore, we repeated the numerical simulations at the critical values of the hopping parameter for $L_t = 2$ and $L_t = 4$, with different temporal lattice extensions and unchanged β, λ. Since we have $L_t \geq 2$, this means that at the $L_t = 2$ point the possible temperatures are $T = 2T_c/n$ with $n \geq 2$. At the $L_t = 4$ point we also have two temperatures above T_c because the possible values are $T = 4T_c/n$. The numerical simulation results for $\delta(T)/T^4$ are shown in figure 7, where vertical error bars refer to the statistical errors from the averages, horizontal ones to the errors due to the uncertainty in the critical hopping parameter, and the shaded areas indicate the error coming from the derivatives $\partial\kappa/\partial\tau$. The latter errors result in overall vertical shifts of the curves. (More precisely, the effect of changing $\partial\kappa/\partial\tau$ is to a good

approximation an overall multiplication, therefore differences as $\log(\delta(T_1)/T_1^4) - \log(\delta(T_2)/T_2^4)$ are better determined than the individual values.) As can be seen, the errors are substantial, especially in the Higgs phase below T_c. In the symmetric phase, where the errors are relatively small, the dominant feature is a rather fast decrease: at $T = 2T_c$ the quantity $\delta(T)/T^4$ is very small, which implies the relation $\epsilon/3 \simeq P$.

It is also interesting to try to extract the derivative $\partial(\delta(T)/T^4)/\partial T$ by changing the hopping parameter κ in a small range around κ_c and keeping the other two bare parameters β and λ fixed. Previous experience [7, 8] and comparison of the present results at points with shifted κ-values, such as m2[12/65] with m2[12/70] and m4[24/35] with m4[24/85], show that the renormalized parameters R_{HW} and $g_R^2(M^{-1})$ change very little. The only substantial change is in the lattice spacing, which can be seen e. g. on the change of the W-mass. We neglect the small changes in R_{HW} and $g_R^2(M^{-1})$ and make the reasonable assumption that the LCP's are parallel in a small κ interval. (That is, the partial derivatives $\partial\kappa/\partial\tau$ etc. appearing in eq. (18) are unchanged.) Thus the derivative $\partial(\delta(T)/T^4)/\partial T$ can be obtained from the derivatives of the global averages $\langle L_{\varphi,x\mu}\rangle$, $\langle Q_x\rangle$ and $\langle P_{pl}\rangle$. The derivatives of these quantities with respect to κ can be determined in numerical simulations by the reweighting technique. Then the derivative with respect to T is given by

$$\left.\frac{\partial}{\partial T_r}\,\frac{\delta(T)}{T^4}\right|_{\kappa=\kappa_c} \simeq -\frac{1}{T_r}\left[\frac{da}{d\kappa}\right]^{-1}\frac{\partial}{\partial\kappa}\frac{\delta(T)}{T^4}\;, \tag{19}$$

where we set the lattice spacing at κ_c to unity and $T_r \equiv T/T_c$. The numerical results from comparing the W-mass at the points m2[12/65] with m2[12/70] and m4[24/35] with m4[24/85], respectively, are

$$\left[\frac{da}{d\kappa}\right]^{-1}_{\rm m2} = 0.00105(10)\;, \qquad \left[\frac{da}{d\kappa}\right]^{-1}_{\rm m4} = 0.000209(17)\;. \tag{20}$$

The obtained estimates of the derivative $\partial(\delta(T)/T^4)/\partial T$ are illustrated in figure 8. Note that at the phase transition point the derivatives are determined in the corresponding metastable phases.

The results of the numerical simulations on $\delta(T)$ will be compared with perturbation theory results in the next section.

5 Comparison with the perturbative predictions

In the previous sections we have presented a quantitative description of the electroweak phase transition for $M_H \simeq 34$ GeV on the lattice. By comparing data from lattice simulations for the SU(2)-Higgs model with the perturbative results, one can hope to identify non-perturbative features and to achieve a better understanding of the electroweak phase transition. Therefore, in this section we shall present a comparison between data of the present lattice results and the perturbative predictions.

We have determined the renormalized masses at zero temperature (M_H, M_W), critical temperature (T_c), jump in the order parameter (ρ), latent heat ($\Delta\epsilon$), and the relation between energy density and pressure. Besides these data, we also include the interface tension (σ) given by [9]. As usual, the dimensionful quantities are normalized by the proper power of the critical temperature.

The most complete perturbative result for the four-dimensional finite temperature electroweak phase transition has been presented in [5, 6]. For increasing Higgs boson mass the perturbative prediction is less and less reliable, since the relative difference between the one-loop and the two-loop perturbative results grows. The deviation strongly depends on the observable: the critical temperature turns out to be quite insensitive to the loop order; however the interface tension receives corrections of $\mathcal{O}(100\%)$ even for $M_H \simeq 34$ GeV.

The present analysis follows the method of [6]. As was mentioned in [6], the treatment of the interface tension has only been performed in the resummation scheme of [5], therefore this scheme will be applied here. In order to make this section self-contained, we recall our convention to treat the high temperature expansion and the renormalization scheme dependence.

The $g^3, \lambda^{3/2}$-potential of [5] involves a high-temperature expansion up to order $(m/T)^3$, which is unsatisfactory for $M_H \simeq 34$ GeV. Thus, we have included all one-loop contributions of order $(m/T)^4$ in our present $g^3, \lambda^{3/2}$-potential. Note, that the numerical evaluation of the one-loop temperature integrals gives a result which agrees with the above approximation up to a few percent.

For the present Higgs boson mass the renormalization scheme dependence is non-negligible. We shall use the scheme suggested by Arnold and Espinosa [3]. It includes the most important zero-temperature renormalization effects and is very close to the on-shell renormalization scheme, which is used by the lattice determination of the masses. Note, that this scheme has been used previously for T_c/M_H in the insert of fig. 15 of ref. [8] and for ρ/T_c, $\Delta\epsilon/T_c^4, \sigma/T_c^3$ and T_c/M_H in ref. [6]. In this scheme the correction to the $\overline{\rm MS}$-potential, used for both the one- and the two-loop results, reads

$$\delta V = \frac{\varphi^2}{2}\left(\delta\mu + \frac{1}{2\beta^2}\delta\lambda\right) + \frac{\delta\lambda}{4}\varphi^4, \tag{21}$$

where

$$\delta\mu = \frac{9g^4v^2}{256\pi^2}, \qquad \delta\lambda = -\frac{9g^4}{256\pi^2}\left(\ln\frac{M_W^2}{\bar{\mu}^2} + \frac{2}{3}\right). \tag{22}$$

Here v is the zero-temperature vacuum expectation value, M_W the W-boson mass at $T = 0$, and the form of the potential at $T = 0$ is

$$V = \frac{\varphi^2}{2}\mu + \frac{\lambda}{4}\varphi^4. \tag{23}$$

Table 8: *Comparison of the normalized latent heat obtained by using the Clausius–Clapeyron equation and the direct lattice formula.*

	$L_t = 2$	$L_t = 4$
$\Delta\epsilon/T_c^4$ from eq. (24)	0.281(19)	0.31(12)
$\Delta\epsilon/T_c^4$ from eq. (15)	0.240(34)	0.28(12)

It is instructive to compare the direct lattice result for the latent heat with the prediction of the Clausius–Clapeyron equation, obtained in perturbation theory [6]:

$$\Delta\epsilon \simeq -\kappa M_H^2 \Delta\rho^2 \ . \tag{24}$$

(The factor κ, instead of the more usual $1/2$, is due to our normalization conventions.) The first line of table 8 shows this, using the lattice results for $\Delta\rho^2$ and M_H^2. The second line contains the latent heat determined in section 3.3. As usual, the numbers in parenthesis denote the errors. The values agree with the prediction of the Clausius–Clapeyron equation within one standard deviation.

Let us compare the lattice results on the jump of the order parameter (ρ), latent heat, interface tension and critical temperature with the perturbative predictions (see fig. 9). For each quantity the dashed lines show the region allowed by the statistical error of a given lattice observable, whereas the dotted lines include an estimate of the systematic error as well. Since the results with largest L_t are closest to the continuum limit, we have plotted them. The statistical errors of the above lattice observables were determined by standard methods. In cases where the $L_t = 2$ result significantly differs from those at larger L_t, rough estimates of the systematic errors can be obtained from these deviations. For the interface tension, where only $L_t = 2$ data exist, the systematic error was estimated from the difference between the results of the "transfer matrix" and the "two-couplings" methods [9]. The last quantity, namely T_c/M_H, will be discussed below.

A rough estimate of the uncertainties of two-loop resummed perturbation theory is given by the difference between the one-loop (shown by triangles on the plot) and two-loop result (shown by squares). In order to represent the region given by this uncertainty we have connected the point of the one-loop result with that of the two-loop result. Comparing to the numerical results, an additional uncertainty arises since neither the Higgs boson mass nor the gauge coupling have been determined exactly. Therefore, the perturbative prediction for an observable at a given order is not one definite value but rather an interval, given by the uncertainties of M_H and g_R. These errors are small. They are represented on the plot by error bars left and right to the triangles and squares, respectively. As a perturbative reference point we will use the

Table 9: *Relation of the critical temperatur T_c and the masses M_H and M_W. For the continuum limit lattice artefacts of order $\mathcal{O}(a^2)$ were considered.*

a	$[2T_c]^{-1}$	$[3T_c]^{-1}$	$[4T_c]^{-1}$	$[5T_c]^{-1}$	$a \to 0$
T_c/M_H	2.026(11)	2.100(33)	2.087(48)	2.21(10)	2.147(40)
T_c/M_W	0.8844(30)	0.898(13)	0.904(19)	0.905(40)	0.910(16)

values $R_{HW} = 0.422(11)$ and $g^2 = 0.585(10)$. We neglect corrections due to the different renormalization conditions used for coupling g_R and the order parameter ρ on the lattice and in the continuum. These corrections are expected to be of relative order g_R^2.

The inspection of figure 9 shows that for the jump of the order parameter, the latent heat, and the interface tension the agreement between numerical simulations and perturbation theory is good. The errors are, however, not small, except for the simulation result for the jump of the order parameter and the perturbative prediction for the latent heat. The interface tension has huge corrections in perturbation theory; nevertheless, the two-loop result agrees with the lattice data. Here one has to note that the perturbative calculation of the interface tension is on different footing, and is up to now less understood, than those of the other quantities. (See e. g. ref. [23].) In case of the ratio of the transition temperature to the Higgs boson mass T_c/M_H, where the results of one-loop and two-loop perturbation theory almost coincide, the numerical simulation results and the extrapolation to the continuum limit are collected in table 9 and shown in figure 10. The errors of the simulations for this quantity are dominated by the uncertainties in the critical hopping parameter discussed in section 3. (This is in contrast to R_{HW} and $g_R^2(M^{-1})$, where these errors cancel to a large extent.) The extrapolated continuum value is $T_c/M_H = 2.147(40)$. The value at $L_t = 2$ is about 5% smaller. This relatively small deviation is better than the expectation based on lattice perturbation theory. For instance, the third paper of ref. [10] gives an estimate of scaling violations of about 20-30% for $L_t = 2$. As figure 10 shows, the value of T_c/M_H extrapolated to the continuum limit differs by about three standard deviations from the two-loop perturbative result. This is under the assumption that the $L_t = 2$ point can be included in the extrapolation, which is supported by the good quality of the fit ($\chi^2 \simeq 1$) and the smallness of scaling violations also discussed in section 2. In our opinion, one cannot exclude the possibility that there are some non-negligible higher-loop contributions and/or non-perturbative effects. These could show up also in other quantities, once the errors there get similarly small.

An interesting new possibility to compare perturbation theory and numerical simulations *as a function of the temperature* is to consider $\delta(T)/T^4$ investigated in the previous section. Since the perturbative calculations also involve a high temperature expansion, in this framework it

is not possible to perform a subtraction at $T = 0$. In the symmetric phase, due to the unsolved infrared problems, perturbation theory is not applicable. In figure 11 the comparison is done for $(\delta(T) - \delta(T_c))/T_c^4$, where $\delta(T_c)$ is taken in the Higgs phase. The agreement is reasonable but not perfect. In fact, one can question the reliability of perturbation theory already at T_c, therefore a subtraction at, say, $T = T_c/2$ would be even safer. In this case the curve in figure 11 is shifted downwards and inside the Higgs phase the agreement becomes good. The discrepacy is then shifted to the point at T_c.

6 Discussion

The results presented in this paper are the outcome of detailed numerical simulations of the thermodynamical properties of the electroweak phase transition in the SU(2) Higgs model at Higgs boson mass $M_H \simeq 34$ GeV.

The high precision data for the correlation functions and Wilson loops were fitted carefully to extract the true statistical errors of the masses and static potential, respectively. We also tried to identify and control the systematic errors such as finite volume effects and lattice artefacts. The former are well under control and we could extrapolate the results to infinite volume reliably. In order to estimate lattice artefacts, we performed the first high statistics numerical simulations with temporal lattice extensions up to $L_t = 5$. As the results show, for interesting physical quantities the deviations between $L_t = 2$ and the maximal investigated L_t are small (see eq. 17, table 8, fig. 10). In general, the size of lattice artefacts turned out to be surprisingly small, in accordance with previous observations concerning $L_t = 2$ and $L_t = 3$ [7, 8]. Therefore, once sufficiently small statistical errors are achieved, the extrapolation to the continuum limit from the range $2 \leq L_t \leq 5$ seems feasible. Note in this respect that our largest errors in some important cases come from the uncertainties in the critical hopping parameters, which are due to the use of 32-bit arithmetics in the simulations.

It is interesting to compare the numerical simulation results to perturbation theory, which is expected to work well at $M_H \simeq 34$ GeV for some quantities (T_c or ρ); however, this Higgs boson mass appears to be at the edge of its domain of validity for other quantities (e.g. $\Delta\epsilon$ or σ). As the discussion in section 5 shows, there is in general a satisfactory agreement within the present accuracy. However, an important discrepancy is observed in the simple quantity T_c/M_H at the level of about 3 standard deviations, which could perhaps hint to higher-order and/or non-perturbative contributions (see figure 10). In fact this quantity is relatively easy to determine with small errors. It is possible that deviations of similar magnitude will emerge in other quantities as well, once the precision becomes similar there.

We also determined the temperature dependence of the thermodynamical quantity $\delta \equiv \epsilon/3 - P$ (ϵ = energy density, P = pressure) in a range $1/4 \leq T/T_c \leq 2$ (see figure 7). In the Higgs phase the errors are relatively large. Within these errors there is a reasonable agreement with perturbation theory. In the symmetric phase, where perturbation theory is plagued

by uncontrollable infrared singularities, δ/T^4 becomes rapidly rather small: at the last point $T/T_c = 2$ it is already almost compatible with zero. Therefore, at higher temperatures we have $\epsilon/3 \simeq P$, as in the photon gas. The knowledge of this thermodynamical equation of state is important in the history of the early Universe.

Acknowledgements

We thank W. Buchmüller, A. Hebecker, K. Jansen, A. Patkós and R. Sommer for discussions. Two of us (F. Cs. and Z. F.) were partially supported by Hungarian Science Foundation grant under Contract No. OTKA-F1041/3-T016248/7.

References

[1] D.A. Kirzhnitz, JETP Lett. 15 (1972) 529;
D.A. Kirzhnitz, A.D. Linde, Phys. Lett. B42 (1972) 471; Ann. Phys. (NY) 101 (1976) 195.

[2] V.A. Kuzmin, V.A. Rubakov, M.E. Shaposhnikov, Phys. Lett. B155 (1985) 36.

[3] P. Arnold, O. Espinosa, Phys. Rev. D47 (1993) 3546.

[4] W. Buchmüller, Z. Fodor, T. Helbig, D. Walliser, Ann. Phys. 234 (1994) 260.

[5] Z. Fodor, A. Hebecker, Nucl. Phys. B432 (1994) 127.

[6] W. Buchmüller, Z. Fodor, A. Hebecker, Nucl. Phys. B447 (1995) 317.

[7] F. Csikor, Z. Fodor, J. Hein, K. Jansen, A. Jaster, I. Montvay, Phys. Lett. B334 (1994) 405.

[8] Z. Fodor, J. Hein, K. Jansen, A. Jaster, I. Montvay, Nucl. Phys. B439 (1995) 147.

[9] F. Csikor, Z. Fodor, J. Hein, J. Heitger, Phys. Lett. B357 (1995) 156.

[10] K. Farakos, K. Kajantie, K. Rummukainen, M. Shaposhnikov, Nucl. Phys. B407 (1993) 356; B425 (1994) 67; B442 (1995) 317;
K. Kajantie, M. Laine, K. Rummukainen, M. Shaposhnikov, CERN preprint, 1995 (hep-lat/9510020).

[11] F. Karsch, T. Neuhaus, A. Patkós, Nucl. Phys. B441 (1995) 629.

[12] E.M. Ilgenfritz, J. Kripfganz, H. Perlt, A. Schiller, Phys. Lett. B356 (1995) 561.

[13] A. Jakovác, A. Patkós, P. Petreczky, Eötvös University preprint, (hep-ph/9510230).

[14] K. Jansen, talk given at the International Symposium on Lattice Field Theory, July 1995, Melbourne, DESY preprint, (hep-lat/9509018).

[15] Z. Fodor, K. Jansen, Phys. Lett. B331 (1994) 119.

[16] B. Bunk, Nucl. Phys. B (Proc. Suppl.) 42 (1995) 566.

[17] C. Michael, A. McKerrell, Phys. Rev. D51 (1995) 3745.

[18] M. Lüscher, Comm. Math. Phys. 104 (1986) 177;
I. Montvay, P. Weisz, Nucl. Phys. B290 (1987) 327.

[19] A. Jaster, PhD thesis, 1995, University of Hamburg.

[20] A.M. Ferrenberg, R.H. Swendsen, Phys. Rev. Lett. 61 (1988) 2635; Phys. Rev. Lett. 63 (1989) 1195.

[21] J. Potvin, C. Rebbi, Phys. Rev. Lett. 62 (1989) 3062;
S. Huang, J. Potvin, C. Rebbi, S. Sanielevici, Phys. Rev. D42 (1990) 2864, errata: D43 (1991) 2056.

[22] R. Gupta et al., Phys. Rev. D36 (1987) 2813.

[23] D. Bödeker, W. Buchmüller, Z. Fodor, T. Helbig, Nucl. Phys. B423 (1994) 171.

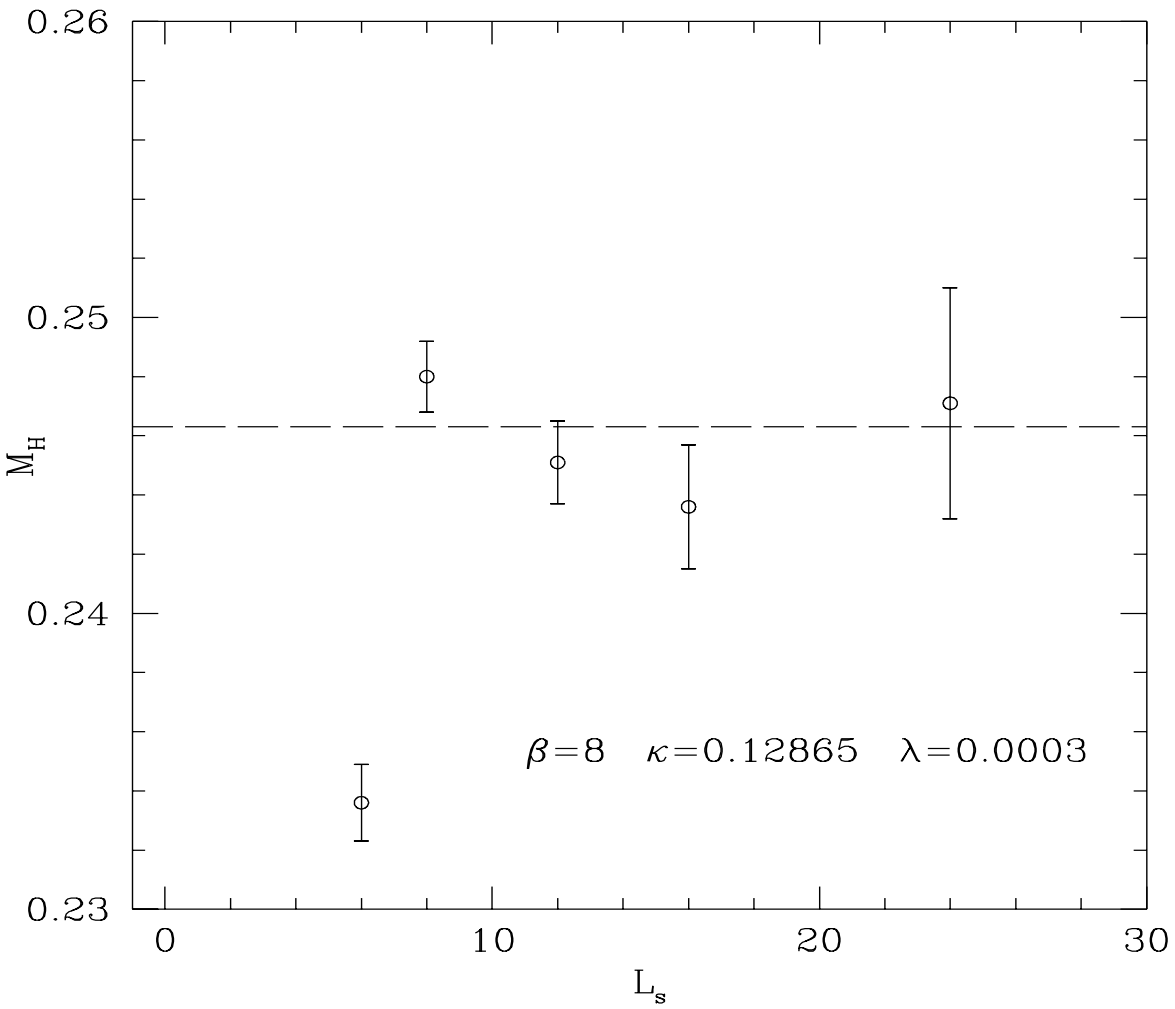

Figure 1: The Higgs boson mass on different volumes. The horizontal line corresponds to $M_H = 0.2463$.

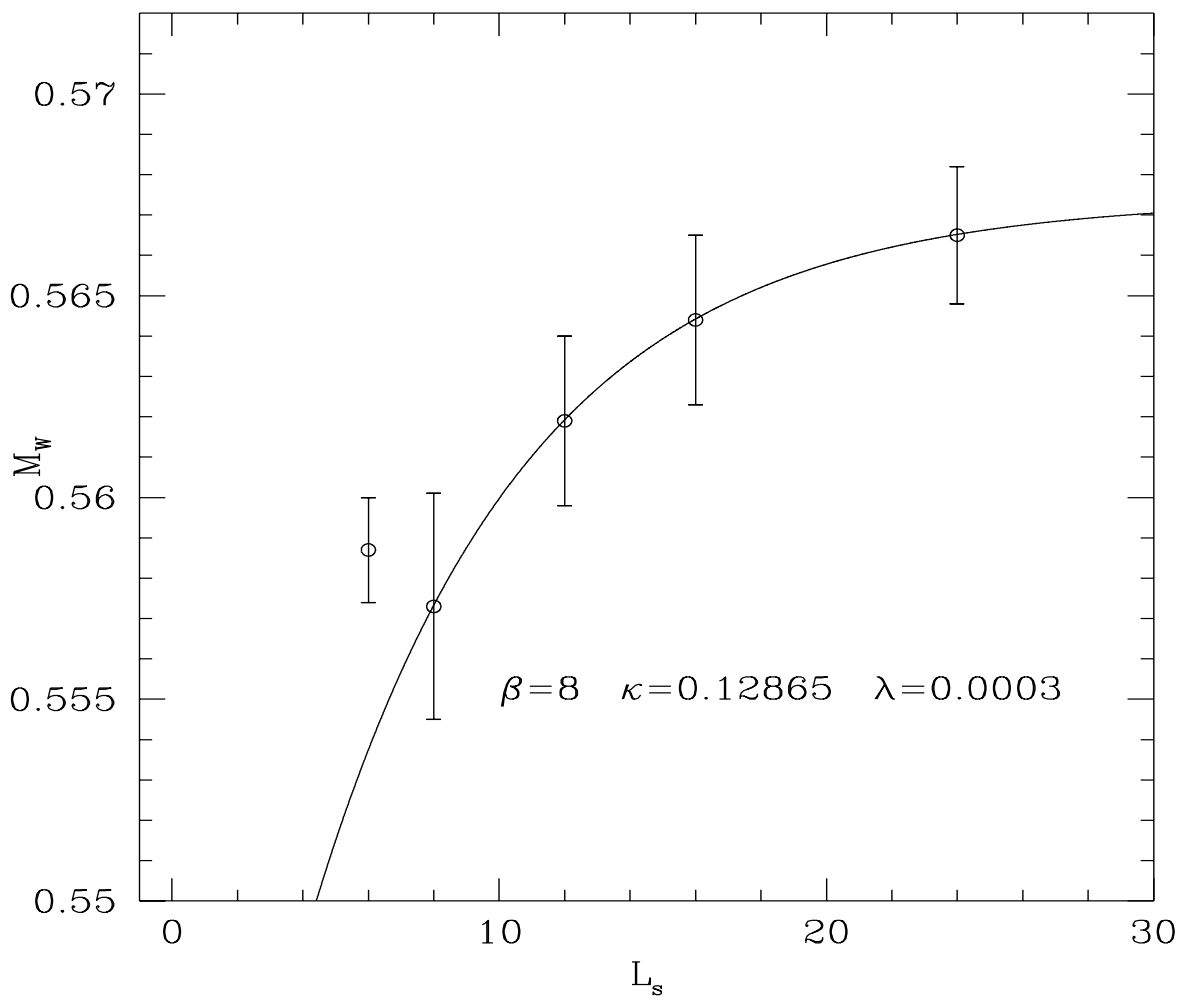

Figure 2: The W-boson mass on different volumes. The curve shows the three-parameter fit $M_W = (1 - 0.06 \cdot \exp(-0.1523 \cdot L_s)) \cdot 0.5674$.

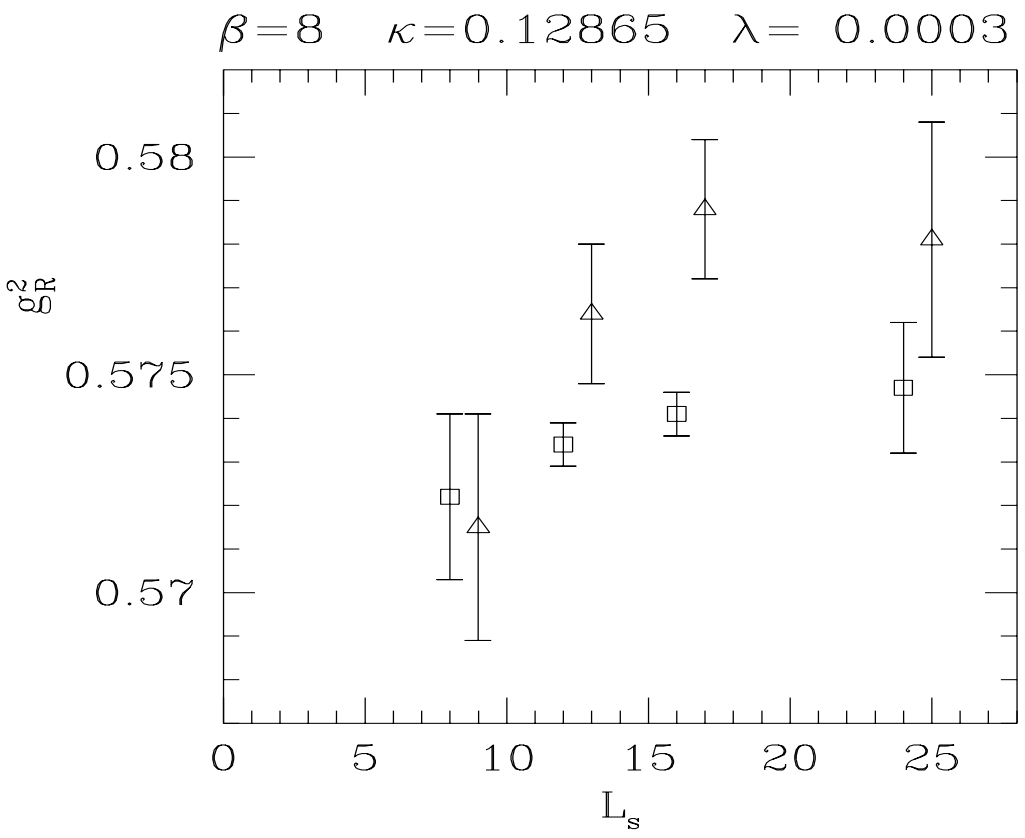

Figure 3: Finite size effects for the renormalized gauge coupling. The squares represent the values obtained by the global definition. The values for the local definition are the triangles, which are slightly displaced for better visualization.

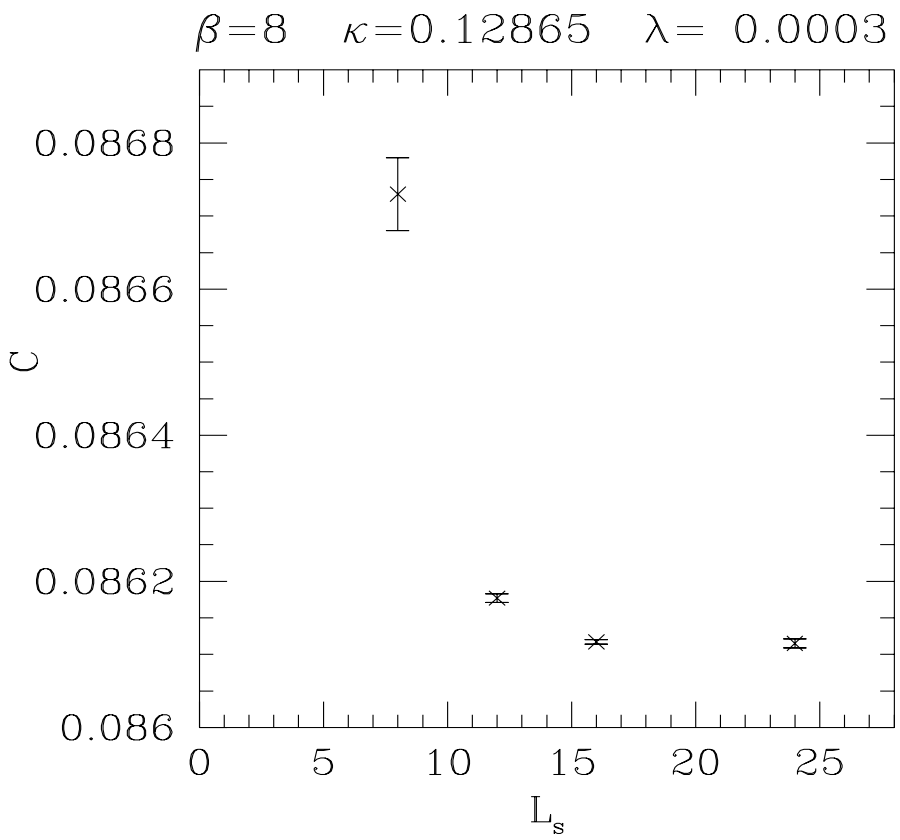

Figure 4: Finite size effects for the constant C in the static potential.

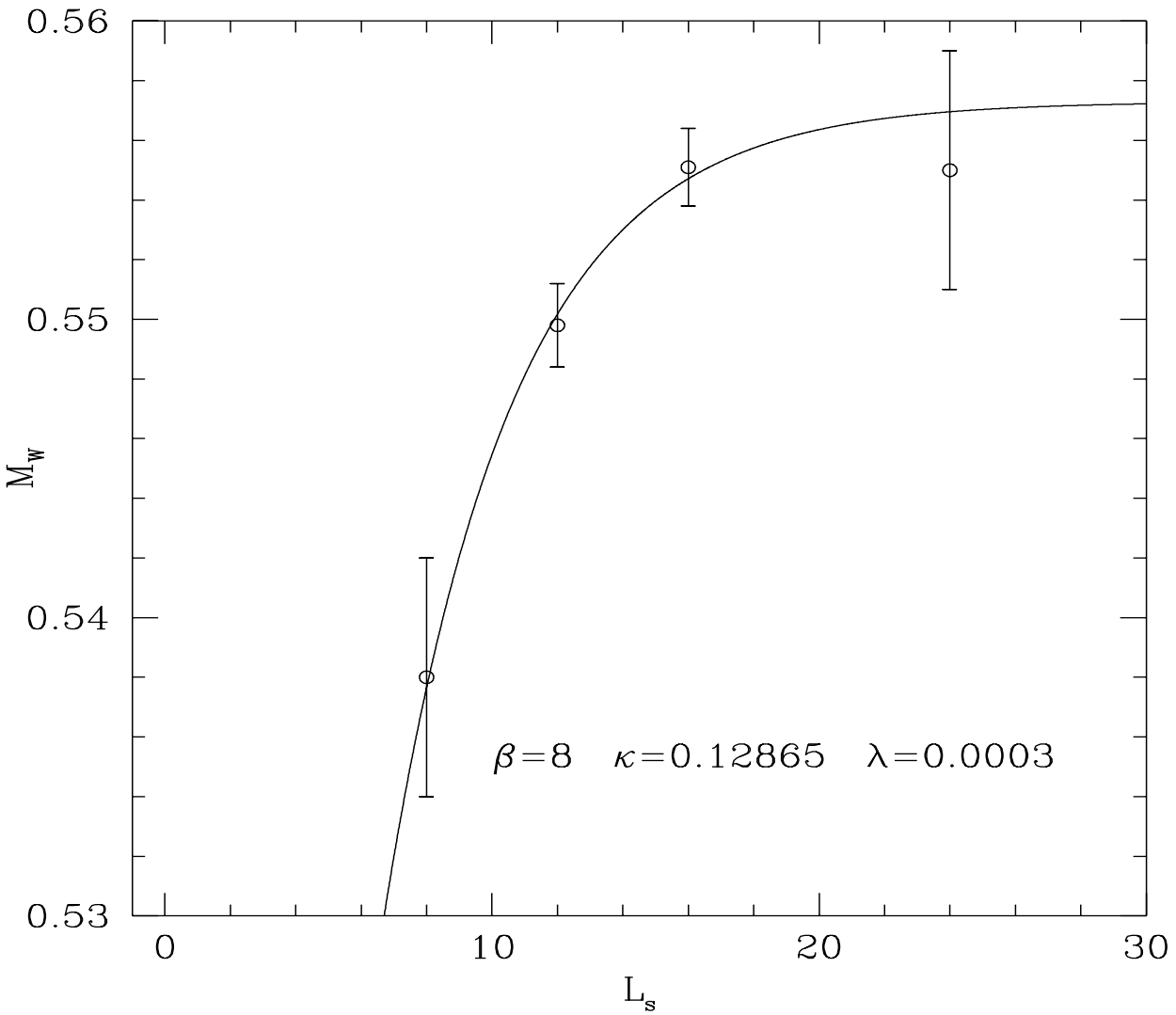

Figure 5: The W-boson mass on different volumes as obtained from the static potential. The curve shown is the three-parameter fit $M = (1-0.2678\cdot\exp(-0.2535\cdot L_s))\cdot 0.5573$.

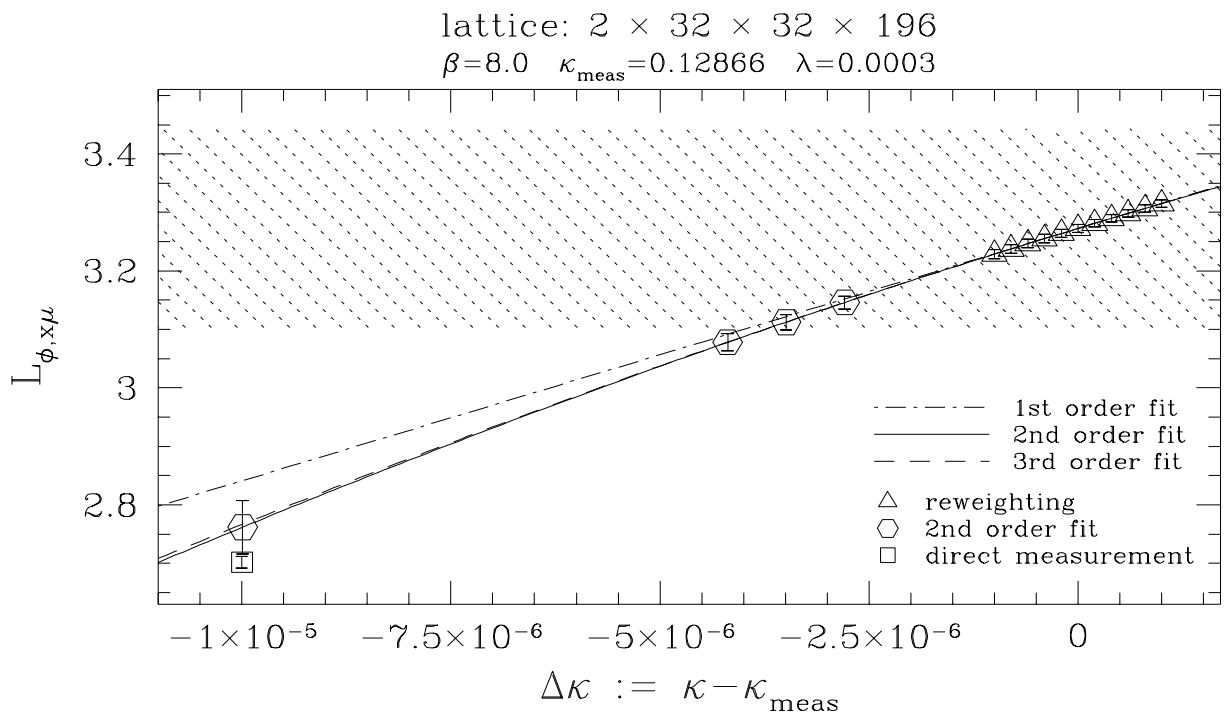

Figure 6: $L_{\varphi,x\mu}$ as a function of κ. The curves are fitted to the data points from the reweighting. To give an impression of the errors some estimates from 2nd order are included. The shaded area gives the variance of $L_{\varphi,x\mu}$ at $\kappa = 0.12866$.

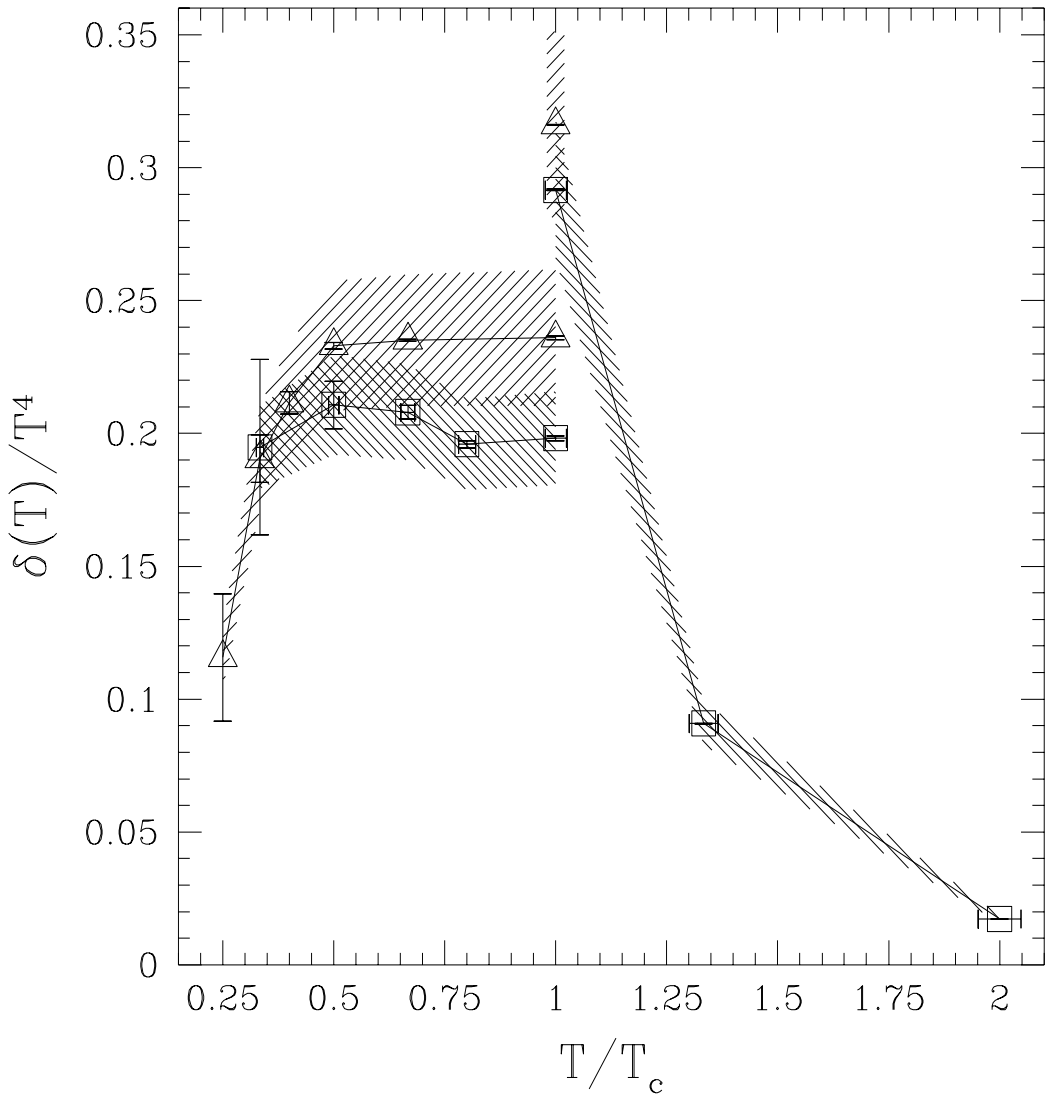

Figure 7: Results of the numerical simulations for $\delta(T)/T^4$ on $L_t = 2$ and $L_t = 4$ lattices. The former are shown by triangles the latter by boxes. The errors are explained in the text.

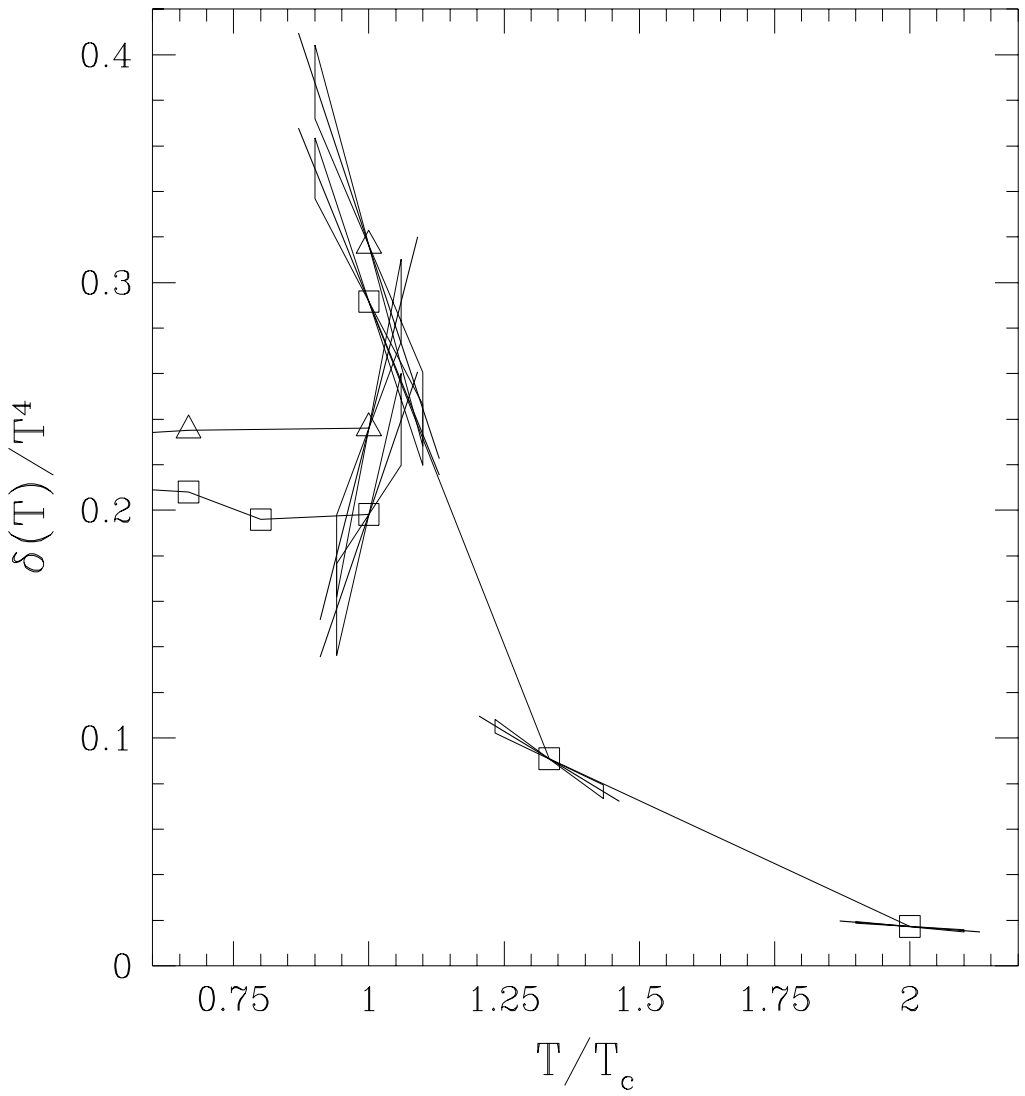

Figure 8: $\delta(T)/T^4$ as a function of T/T_c together with $\partial(\delta(T)/T^4)/\partial T$. The straight lines represent the tangents as calculated by the method described in the text (their lengths have no significance). For $T/T_c < 1$ the results on the derivatives are consistent with zero, and are not shown. The elongated triangles around the straight lines indicate the errors of the tangents.

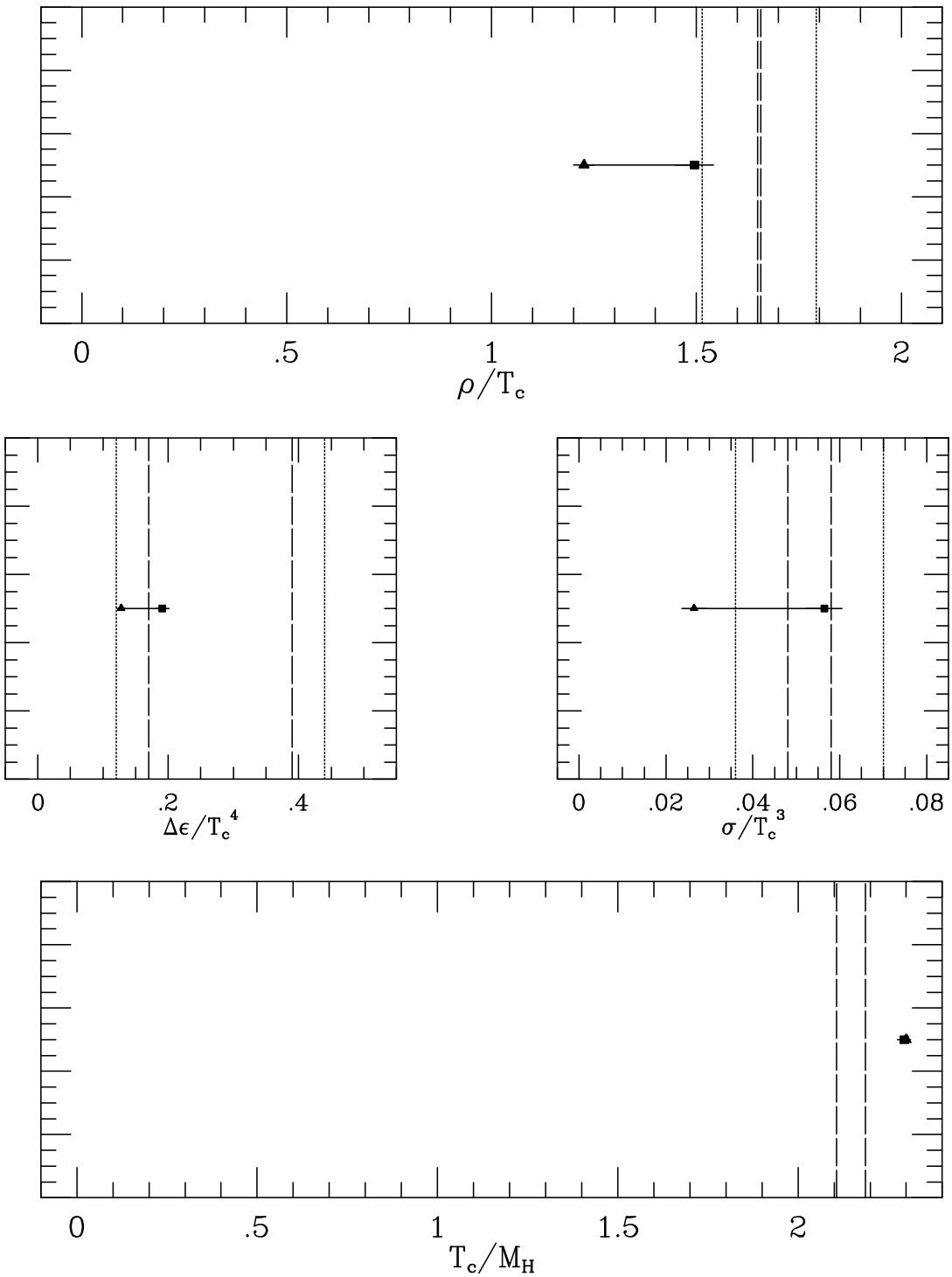

Figure 9: Comparison of the numerical simulation results with those from two-loop resummed perturbation theory. Vertical strips give the numerical results with errors. The triangles are the perturbative predictions at order g^3, the boxes those at g^4.

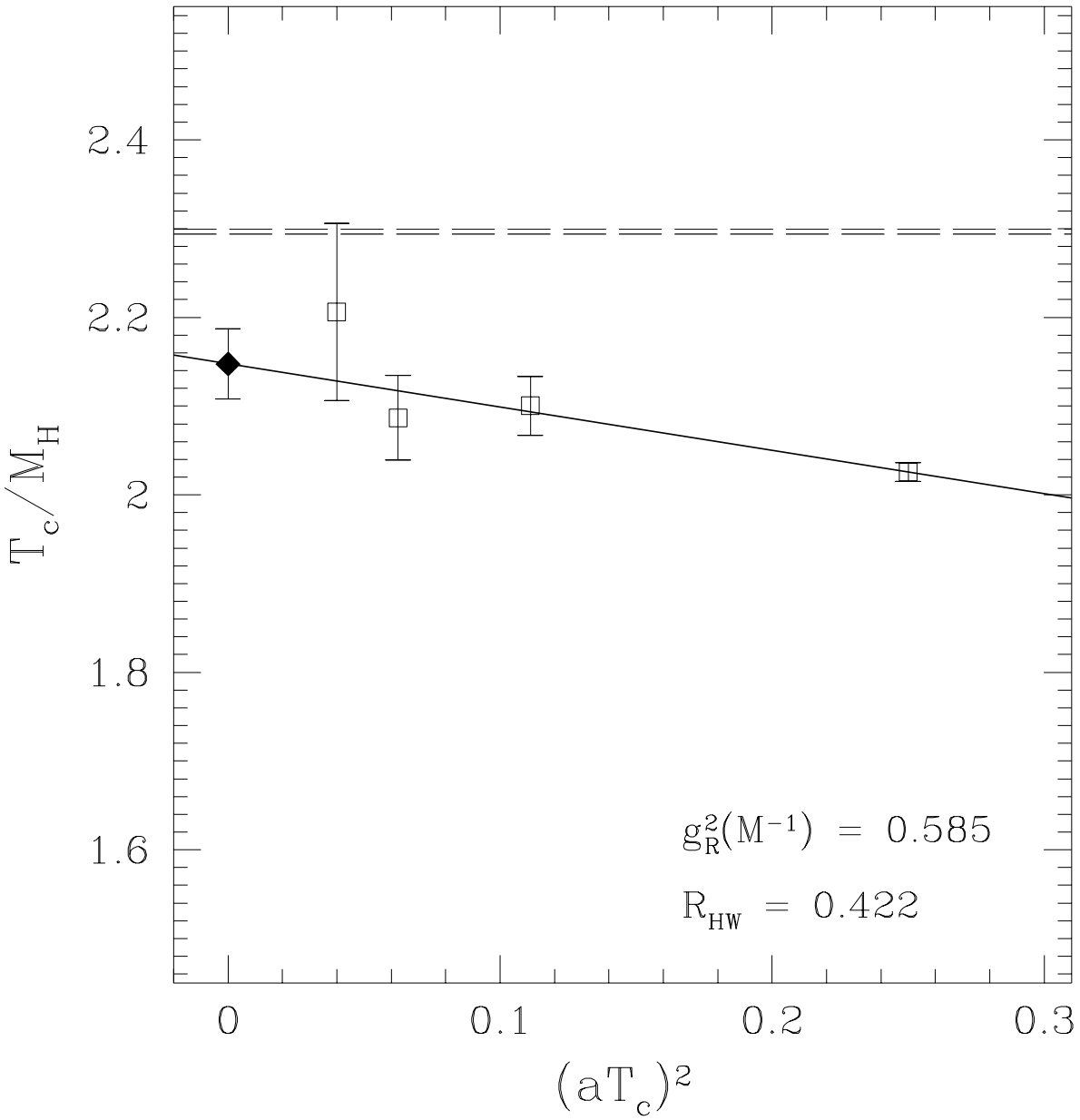

Figure 10: The numerical results for the ratio of the transition temperature and the Higgs boson mass T_c/M_H versus $(aT_c)^2 = L_t^{-2}$. The straight line is the extrapolation to very small lattice spacings, which gives the continuum value shown by the filled symbol. The dashed horizontal lines are the perturbative predictions at order g^3 (upper) and g^4 (lower), respectively.

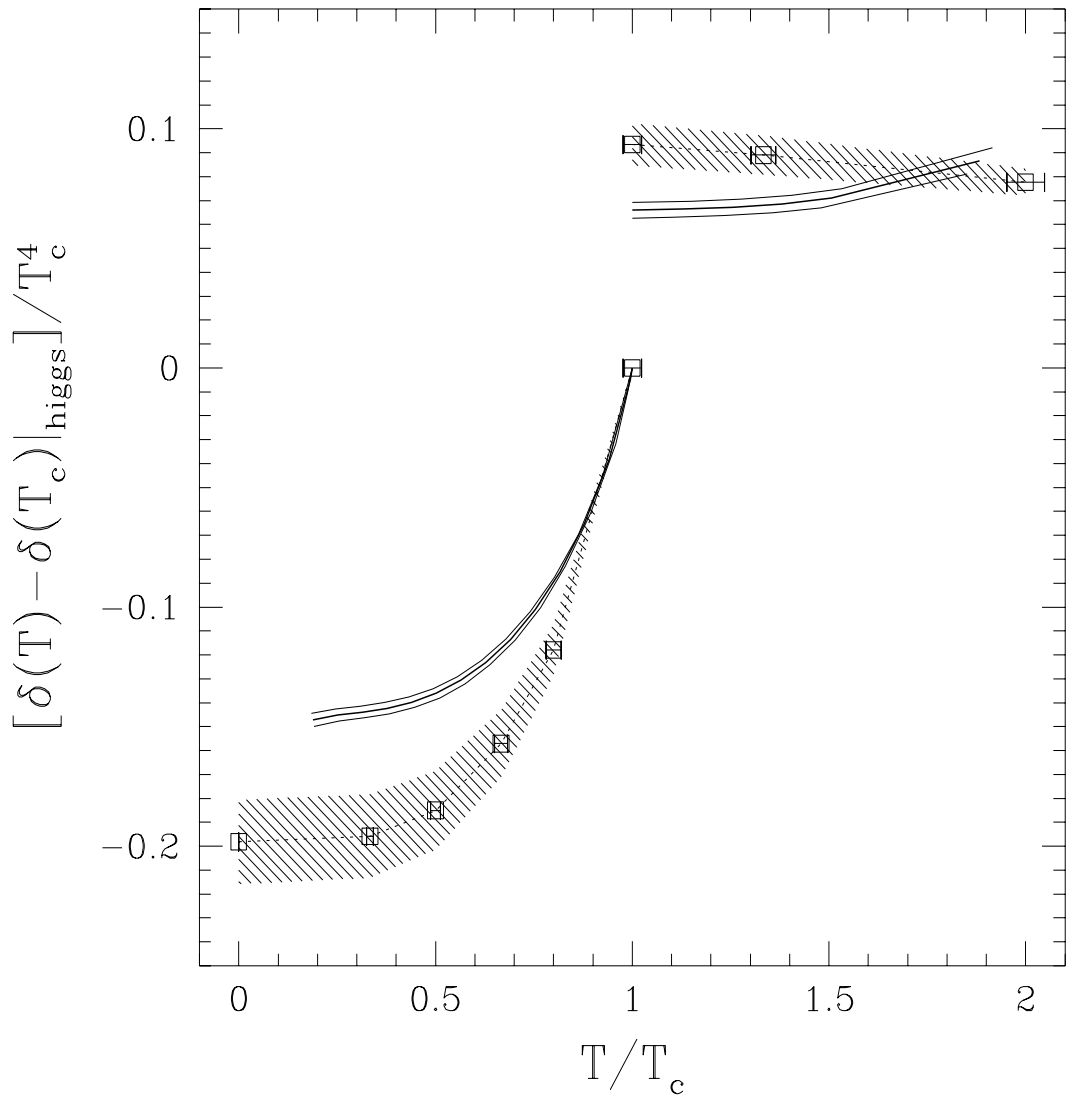

Figure 11: Comparison of the numerical results for $\delta(T)$ with those from two-loop perturbation theory. The shaded areas show the uncertainty of the numerical simulation results due to the uncertainty in the derivatives of bare parameters along the lines of constant physics. The solid lines show the perturbative results together with the uncertainties induced by the errors on R_{HW} and g_R^2.